J Mater Sci (2007) 42:1649–1659
DOI 10.1007/s10853-006-0967-x

Processing and properties of ultrafine-grain aluminum alloy 5005 sheet

R. Lapovok · P. W. J. McKenzie · P. F. Thomson · S. L. Semiatin

Received: 8 May 2006 / Accepted: 12 September 2006 / Published online: 16 December 2006

Abstract The potential of ECAP sheet machine build in Monash University to refine the grain size, enhance mechanical properties, and improve deep drawability of the sheet was investigated for a representative aluminum alloy, AA5005. The annealed sheet was subjected to one, two, or four ECAP passes through 90º using route A or route C followed by annealing at 400 °C for 15 min. It was established that only one ECAP pass is required to obtain a significant improvement in both normal and planar anisotropy. A subsequent annealing enabled the recovery of ductility of the material lost during ECAP while maintaining the improved plastic anisotropy.

Introduction

Equal channel angular pressing (ECAP) is a well-known method of severe plastic deformation to obtain ultrafine-grain materials with significantly improved mechanical properties such as strength and ductility [1]. To the present, ECAP has been restricted essentially to the treatment of bulk billets of square or circular cross-section with limited size. The tendency for buckling and the large increase in the surface-area-to-volume ratio, which increases frictional forces, have hindered its application to sheet metals. However, the demand for aluminium materials with a combination of high strength and good ductility is especially high for sheet applications in the aerospace and automotive industries. One of the specific features of the ECAP process justifying its high value for sheet applications is that it can be used to control the size and distribution of second-phase precipitate particles that provide strengthening [2]. The combination of high formability with strengthening during the paint-bake cycle is widely sought in production of aluminium panels for aircraft and automobile bodies.

There is evidence that the heavy shear developed during *asymmetric* rolling is effective in increasing the coefficient of normal plastic anisotropy [3, 4]. Previous investigations of aluminum alloy (AA) 6111 sheet have shown that the simple shear introduced into a material by ECAP has a similar effect [2]. In this previous work, the room temperature ductility was enhanced by approximately 25%, and the coefficient of normal plastic anisotropy increased from 0.6 to 1.3, consequently enhancing deep drawability. However, due to large frictional forces and problems in scale-up, the ECAP process is not well suited for the processing of sheet material. Hence, ECAP of sheet material has not been commercialized to date.

To overcome the challenges associated with the continuous severe-plastic deformation of aluminum sheet using conventional ECAP tooling, a unique machine (Fig. 1) has been commissioned at Monash University. Problems associated with friction and buckling are overcome by its innovative design.

R. Lapovok (✉) · P. W. J. McKenzie · P. F. Thomson
Materials Engineering Department, Monash University, Clayton, Victoria 3800, Australia
e-mail: rimma.lapovok@spme.monash.edu.au

S. L. Semiatin
Air Force Research Laboratory, Materials and Manufacturing Directorate, AFRL/MLLM, Wright-Patterson Air Force Base, OH 45433-7817, USA

Fig. 1 Machine for ECAP of aluminum sheet at Monash University

Table 1 Bulk chemical analysis of AA5005 program material (in weight percent)

Al	Mg	Cu	Mn	Fe	Si	Zn	Cr
>95	0.5–1.1	0.2	0.2	0.7	0.3	0.25	0.1

Furthermore, the equipment can be readily scaled for different widths of aluminium sheet and, potentially, for processing other sheet materials. In the present work, the application of the specialized ECAP equipment to refine the grain size in a representative aluminum sheet alloy (5005) is demonstrated, and the resulting improvements in formability, the associated textures, and mechanical properties are summarized.

Material and procedures

The program material comprised AA5005 purchased in the form of 2-mm-thick sheet. The bulk chemical analysis of the as-received material is summarized in Table 1. As revealed by optical microscopy (Fig. 2a), the as-received material had an initial grain size of 77 ± 27 μm.

Strips for ECAP processing measuring 2000 mm in length and 90 mm in width were cut from the sheet in the rolling direction and annealed at 540 °C for 15 h followed by furnace cooling. The annealed sheet was subjected to one, two, or four ECAP passes through 90° using route A (no rotation of the sheet between passes) or route C (180° rotation about RD direction between passes) with a strain-rate of 0.01 s^{-1}.

The microstructures of the starting (annealed) and deformed materials were determined on longitudinal cross sections via optical microscopy and transmission-electron microscopy (TEM), the latter using Philips EM420 and CM20 microscopes operated at 100 and 200 kV, respectively. For this purpose, TEM foils were prepared using a twin jet Streuers Tenupol-5 electropolishing unit and a solution of 33% nitric acid in methanol at 30 V, ~200 mA, and a bath temperature of –20 °C. Bright-field (BF) images and selected-area diffraction (SAD) patterns (with an aperture size of 1.1 μm) were taken for analysis.

The mechanical properties of material subjected to various numbers of passes were characterized via uniaxial tension testing in an Instron (Micro-Tester) 5848 machine and a small-scale Swift (flat-bottom) cup test. All tests were performed in triplicate. The tension tests were conducted at a strain rate of 0.01 s^{-1} using samples cut along the longitudinal (L), transverse (T), and diagonal (45°) directions. The normal plastic anisotropy (r value) was determined for each tensile test according to the procedure in ASTM Standard E 517-00. The Swift test used a 6 mm diameter punch and round disks of various diameters (between 9.5 and

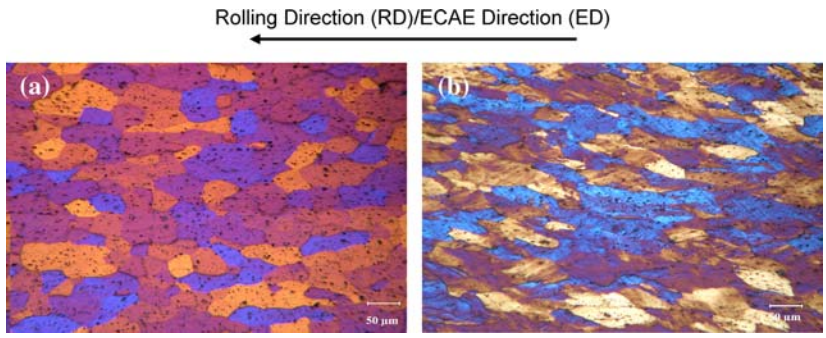

Fig. 2 Optical microstructures taken on longitudinal cross sections: (**a**) after annealing at 540 °C for 15 h and (**b**) after 1 ECAP pass

14.6 mm) which had been ground and polished to the required thickness of 0.4 mm using Tenupol-1 equipment.

The plastic anisotropy and drawing behavior were interpreted in the context of the textures developed in as-deformed and deformed-and-annealed conditions. To this end, partial ($0 \leq \chi \leq 80°$) pole figures (PFs) for the (111), (200), and (220) planes were determined using in-plane samples and a GBC-MMA texture goniometer with a CuK_α anode and a poly-capillary beam enhancer that collimates the X-ray beam to a 10×10 mm cross-section. The diffracted X-rays were detected in reflection mode. Without imposing sample symmetry conditions, the spherical harmonics method was used with the partial pole figures to obtain orientation distribution functions (ODFs) from which complete {111} pole figures were obtained. These pole figures were subsequently represented in accordance with an idealized negative simple shear model for ECAP deformation, where the ideal orientations and fiber textures for ECAP of FCC materials processed through any die angle has already been developed by Li et al. [5, 6]. To aid in the interpretation of ECAP texture characteristics, the Euler angles for the main ideal orientations after one ECAP pass when the processing angle is 90° are given in Table 2. Here the ED and RD are coincidental and the sense of all reference directions were consistently maintained.

Results and discussion

Optical microstructures

The microstructures of the as-annealed aluminium alloy 5005 material and material after one ECAP pass are shown in Fig. 2. During ECAP, the equiaxed grains of the annealed material (Fig. 2a) became elongated along the theoretical shear direction at an angle of ~26° with the sheet plane (Fig. 2b).

Microstructure evolution—TEM

Microstructure after annealing at 540 °C for 15 h

Figure 3 shows TEM BF images of two grains and the high-angle grain boundary (HAGB) between them for material that had been annealed at 540 °C for 15 h. Apart from the relatively high density of networked dislocations adjacent to the HAGB, the presence of an incoherent equilibrium second-phase at the boundary and within the grains was observed. In addition to the identification of this phase through SAD patterns, the morphology (plates and laths), size (~0.1 to ~0.3 μm), and location within the matrix indicated that this phase is in-fact the stable β-Mg_5Al_8 (formerly Mg_3Al_2) phase [7]. Electron energy dispersive X-ray spectroscopy (EDXS) confirmed this conclusion. The incoherency of this face-centered cubic (fcc) precipitate and the orientation relationship with the surrounding matrix ($(111)_\beta \| (001)_\alpha$; $[110]_\beta \| [010]_\alpha$), indicated that this phase could potentially be very effective in impeding dislocation motion during subsequent ECAP. However, the small relative volume fraction of this phase (<1%) and therefore large mean free path between the precipitates suggested that dislocation motion during ECAP would be relatively uninhibited and only small heterogeneities (whose exact size would be dependent on the precipitate size) would be expected around the particles.

Microstructure after one ECAP pass

To best illustrate the microstructure observed after one ECAP pass, TEM BF images viewed along the <110> zone axes were taken at randomly chosen positions

Table 2 Main ideal orientations and fibers for one ECAP pass of FCC materials processed through a 90° angle, [5, 6]

Notation	Euler angles (°)[a]			Miller indices			Fiber it belongs to φ_3
	φ_1	φ_2	φ_3	ND (approx.)	φ_1	φ_2	
$A^*_{1\theta}$	80.26/260.26	45	0/90	[81 $\bar{1}$]	[1 $\bar{4}$4]	[011]	$\{111\}_\theta$
	170.26/350.26	90	45				
$A^*_{2\theta}$	9.74/189.74	45	0/90	[1 $\bar{4}$4]	[81 $\bar{1}$]	[011]	$\{111\}_\theta$
	99.74/279.74	90	45				
A_θ	45	35.26	45	[914]	[111 $\bar{5}$]	[$\bar{1}$12]	$\{111\}_\theta$,$<110>_\theta$
A_θ	225	35.26	45	[$\bar{1}\bar{1}$15]	[$\bar{9}\bar{1}\bar{4}$]	[$\bar{1}$12]	$\{111\}_\theta$, $<110>_\theta$
B_θ	45/165/285	54.74	45	[15 4 11]	[726 $\bar{1}$9]	[$\bar{1}$11]	$<110>_\theta$
B_θ	105/225/345	54.74	45	[$\bar{7}\bar{2}$619]	[$\bar{1}\bar{5}\bar{4}$11]	[$\bar{1}$11]	$<110>_\theta$
C_θ	135/315	45	0/90	[334]	[22 $\bar{3}$]	[$\bar{1}$10]	$<110>_\theta$
	45/225	90	45				

[a] Given in the $\varphi_2 = 0°$, 45° and 90° sections only

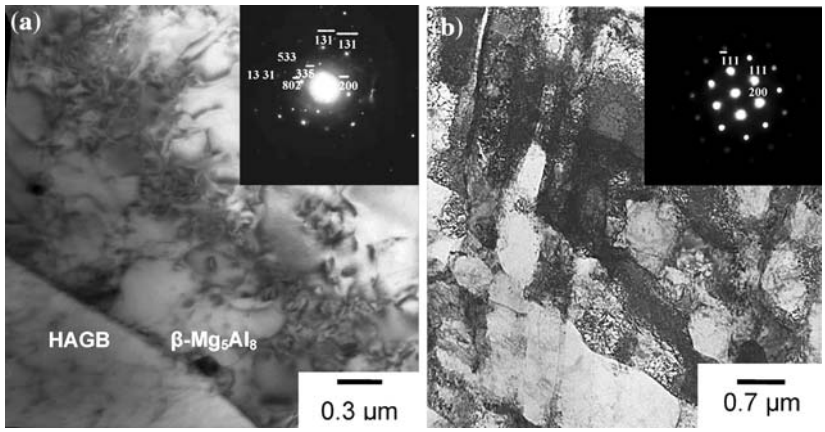

Fig. 3 TEM BF images of the microstructure of AA5005 after. **a**—annealing at 540 °C for 15 h; **b**—one pass of ECAP

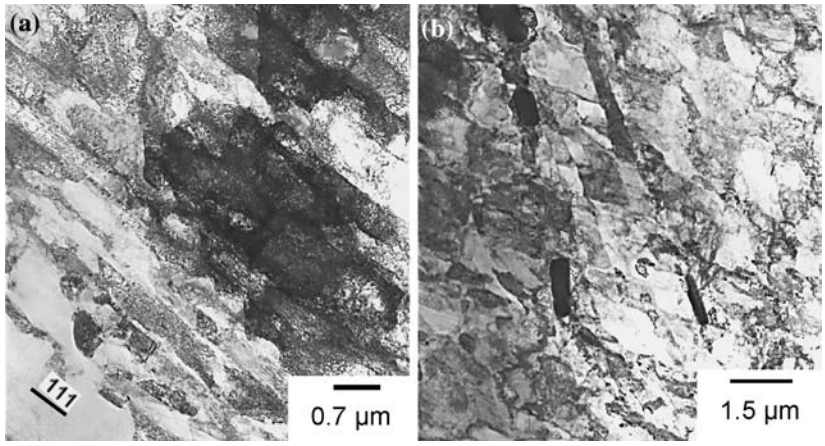

Fig. 4 TEM BF images of the microstructure of AA5005 after one ECAP pass at RT: (**a**) parallel lamellar boundaries containing dislocation cell structures and (**b**) constituent particle alignment with the shearing direction

(Fig. 4). The microstructure appeared to consist primarily of parallel lamellar boundaries (LBs) containing elongated dislocation cell structures with a breadth of ~0.4 μm. The cell boundaries were mainly low angle and orientated along the trace of 111 planes (labeled '111' in Fig. 4a.) Because the 111 planes contain 110 directions and the lamellar boundaries were within an angle of ±15°, the boundaries were parallel to the 110 shear direction, indicating that the major {111}<110> slip systems for fcc materials were indeed operative during a single pass of ECAP. Due to the relatively large equivalent strain imparted to the material per pass (~1.15), this is to be expected. Furthermore, the dislocation cell structure after one pass of ECAP was found to have an approximate mean spacing of 0.6 μm. Some evidence of microband formation was also noted (Fig. 3b), with a 35–65° misorientation with respect to the LBs. The microband and lamellar boundaries displayed low angles (2–4°) of misorientation.

Lower magnification TEM images (Fig. 4b) also revealed an alignment of the large constituent particles after one ECAP pass. In some cases, these particles had a thickness greater than the LB width creating a local distortion of the matrix around the particles. This microstructural feature has also been observed in bulk-processed AA6111 sheet [2]. Interestingly, no particle fragmentation was observed, suggesting that more than one ECAP pass would be required to break-up constituent particles of this size (which varied from ~0.1 to ~0.7 μm) in AA5005.

Microstructure after two ECAP passes

Figure 5 shows TEM BF images of AA5005 subjected to two ECAP passes using route A (Fig. 5a) or route C (Fig. 5b). Because route A involves no rotation of the sample between pressings (and the shear strain is applied at 90° between each successive pass) and route C involves a rotation of 180° about the RD between pressings (for which a redundant strain exists after every two passes), a strongly elongated LB structure was a dominant microstructural feature developed in material processed via route A, but not in route C. However, it is important to point out that the LB

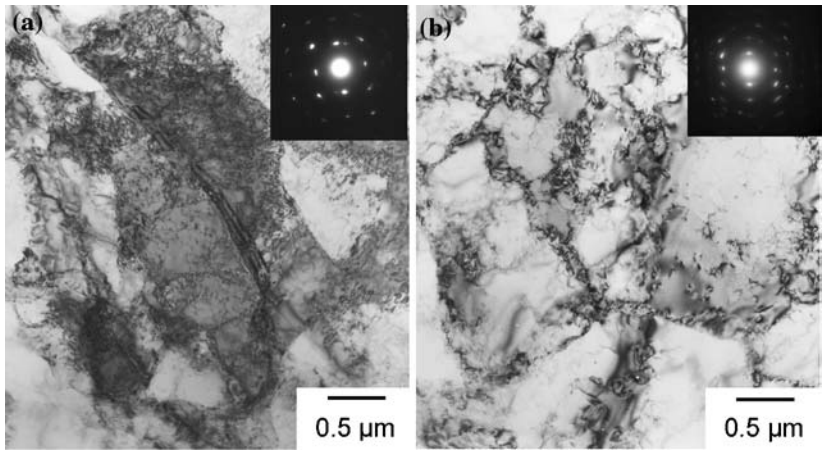

Fig. 5 TEM BF images of the microstructure of AA5005 after two ECAP passes at RT via: (**a**) Route A or (**b**) route C

structure is most easily observed on a plane perpendicular to that viewed here. In addition, the LB structure and dislocation cell/subgrain structure is generally larger in this plane of view [8]. Compared with the microstructure developed during one ECAP pass, the second pass via both routes produced an increase in misorientation angle between the dislocation cell/subgrain boundaries (indicated by the spreading of the diffraction spots in the SAED patterns), albeit with the majority of the dislocation cell/subgrain boundaries still consisting of low misorientations. The average dislocation cell/subgrain size was measured to be almost the same for both routes within experimental error (Table 3).

Microstructure after four ECAP passes

Figure 6 shows TEM BF images of AA5005 subjected to four passes of ECAP using route A (Fig. 6a) or route C (Fig. 6b). The SAED patterns indicated that there was a significantly larger fraction of high misorientation boundaries than after one or two ECAP passes.

From the BF images, it appeared that the dislocation cell/subgrain structures had become more equiaxed most likely because the previous lamellar boundaries had been partially truncated by the operation of multiple slip systems. Nevertheless, LBs still existed, particularly after four ECAP passes using route A. The average size of the dislocation cells/subgrains was almost the same for both routes (Table 3), in spite of the fact that they were more equiaxed after four passes via route C.

Table 3 Average dislocation cell/subgrain size (nm) as a function of the number of ECAP passes

ECAP Route	Number of ECAP passes		
	1	2	4
A	599 ± 215 nm	587 ± 156 nm	350 ± 128 nm
C		591 ± 246 nm	438 ± 150 nm

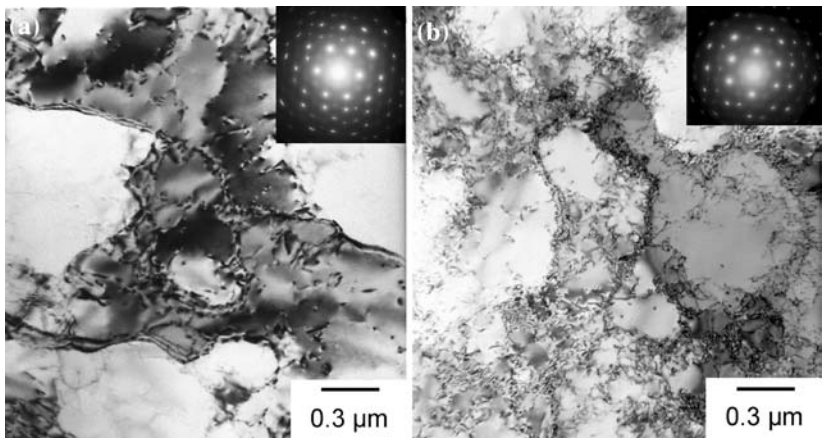

Fig. 6 TEM BF images of the microstructure of AA5005 after four ECAP passes at RT via: (**a**) Route A or (**b**) route C

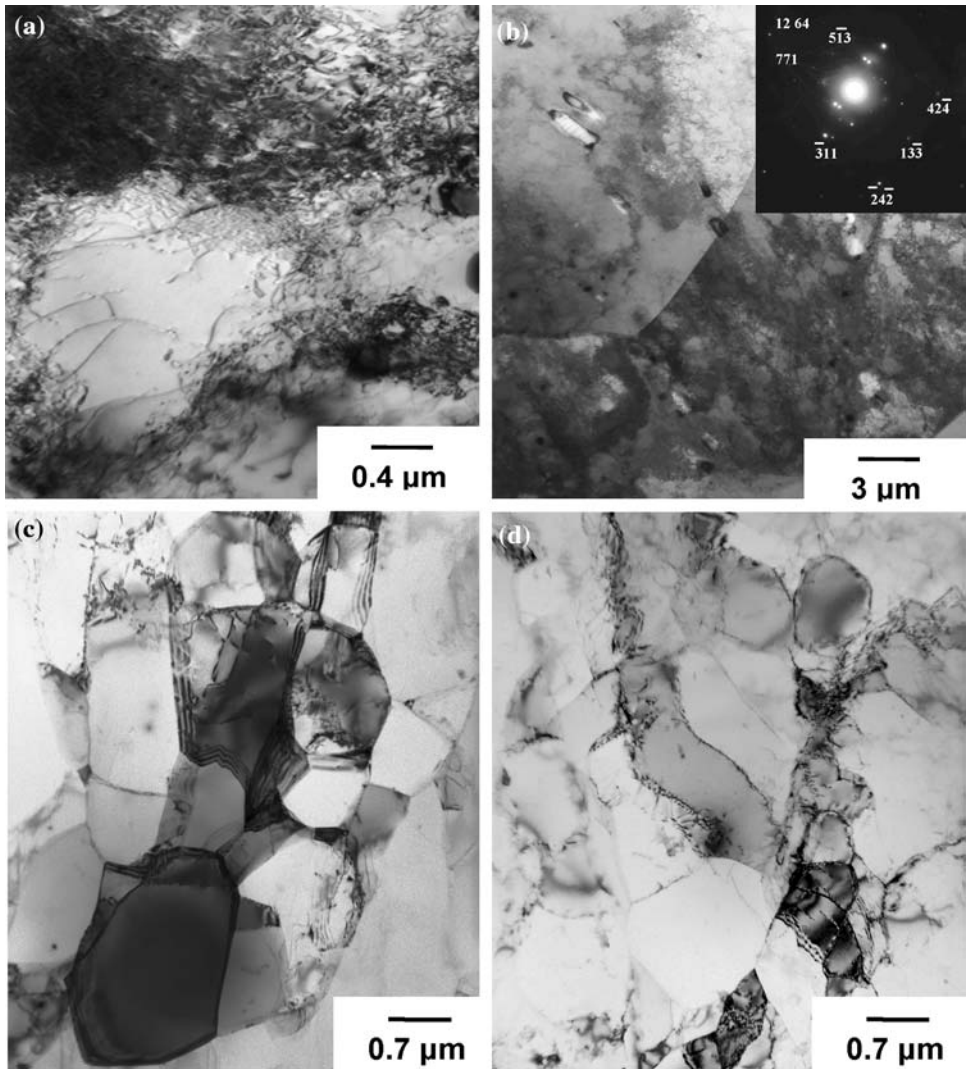

Fig. 7 TEM BF images of the microstructure developed in AA5005 samples by ECAP following by annealing at 400 °C for 15 min: (**a**, **b**) One ECAP pass, (**c**) four ECAP passes via route A, and (**d**) four ECAP passes via route C

Microstructure after one and four ECAP passes followed by annealing

Figure 7a,b shows TEM BF images of the partially recrystallized structure obtained in a one-pass ECAP sample given a short (15-min) anneal at 400 °C. Compared to the undeformed (annealed) material, which had a grain size of 80 ± 40 μm (Fig. 2a), the ECAP'ed-and-annealed material had a mean grain size of ~15 μm. This finer grain size was produced by dislocation rearrangement and annihilation that reduced the overall dislocation density. However, the short-time anneal still left unrecrystallized regions with a high dislocation density. In such areas, it appeared that the stable, incoherent β-Mg_5Al_8 phase particles impeded local dislocation rearrangement and boundary migration during annealing (Fig. 7b). The level of strain imparted into the material after four ECAP passes was sufficiently high to complete recovery and initiate discontinuous recrystallization during the short anneal at 400 °C for both routes (Fig. 7c, d).

Tensile behavior

Stress–strain curves

The results of uniaxial tension tests on the starting (annealed) material and ECAP-deformed specimens are summarized in Fig. 8. Comparison of these engineering stress–strain curves shows that one ECAP pass introduced a severe-plastic deformation in the sheet leading to an increase in stress–strain curves of ~35% and a decrease in ductility from 20–27% (prior to ECAP) to 6–8% (after ECAP). In addition, Fig. 8a, b reveals that the anisotropy in the ductility in the L, T, and D directions was significantly reduced after one

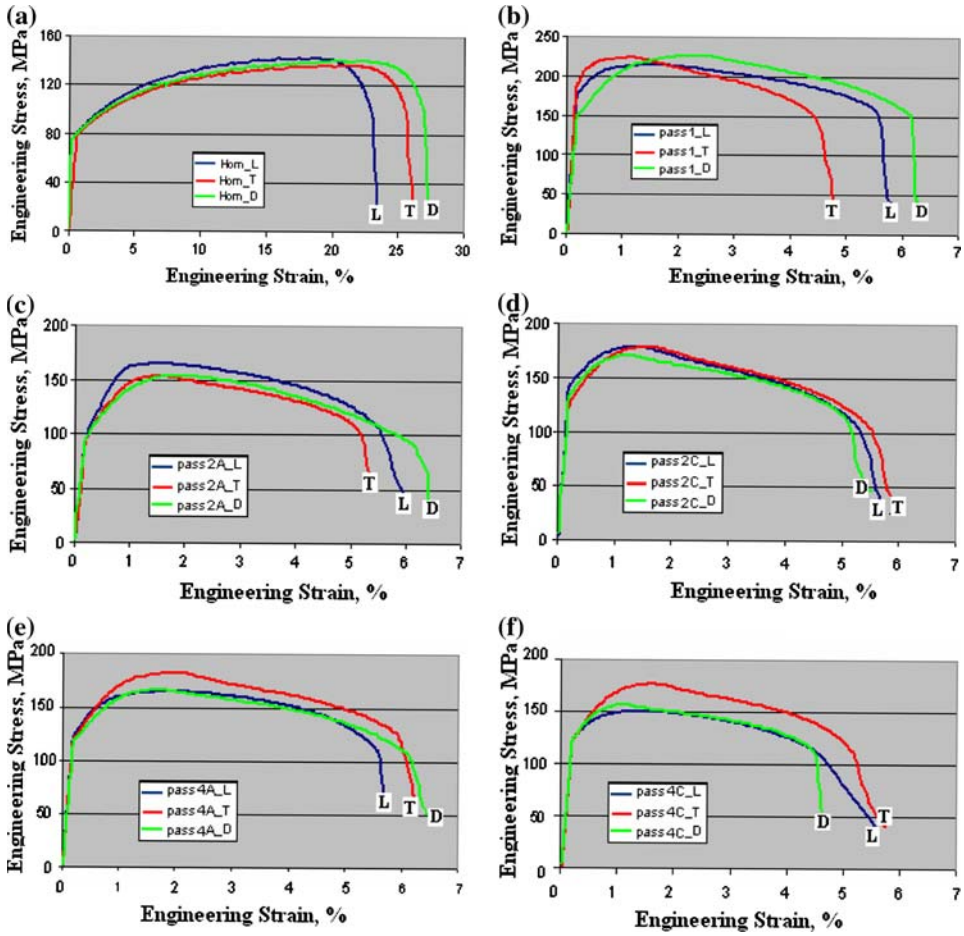

Fig. 8 Engineering stress–strain curves for AA5005: (**a**) Annealed at 540 °C for 15 h, (**b**) after one ECAP pass, (**c**) after two ECAP passes via route A, (**d**) after two ECAP passes via route C, (**e**) after four ECAP passes via route A, and (**f**) after four ECAP passes via route C

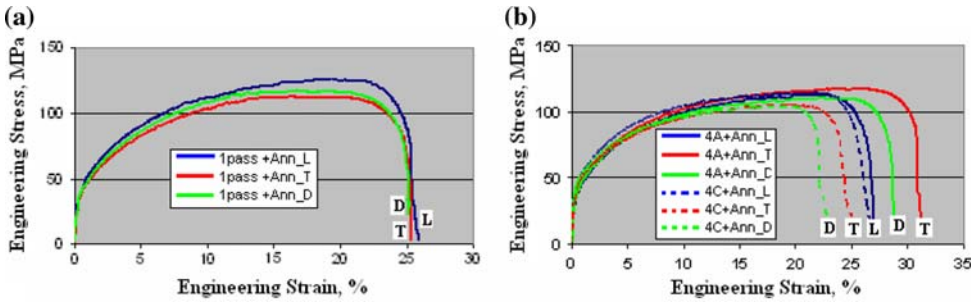

Fig. 9 Engineering stress–strain curves for AA5005 following ECAP and annealing at 400 °C for 15 min: (**a**) One ECAP pass or (**b**) four ECAP passes via routes A or C

pass. Each of the one-pass flow curves also indicated a very short hardening transient followed by quasi-stable flow, thus suggesting that the modest tensile ductility obtained following ECAP was largely due to the rate sensitivity of the flow stress (*m* value). Two- and four-pass ECAP each led to similar *lower* flow stresses, albeit nearly the same ductility, compared to the one-pass results. The lower flow stresses may have one of two sources. The first is the possible reduction of dislocation tangles and the generation of a more-highly recovered structure after two or more ECAP passes. The second possibility is the dissolution of second-phase precipitates with increased number of passes.

Stress–strain curves obtained on material deformed one or four passes and given the short-time, high-temperature anneal (400 °C/15 min) (Fig. 9) indicated that the tensile ductility and strength were similar to the starting material (Fig. 8a). The tensile properties were essentially the same along all three test directions for the material subjected to only one ECAP pass. No improvement in tensile properties was obtained by increasing the number of passes prior to annealing.

Table 4 Normal and planar anisotropy measurements[a]

Condition	r_0	r_{45}	r_{90}	$\bar{r}$	Δr
Annealed 540 °C/15h	0.39	0.48	0.78	0.53	0.21
1 ECAP pass	0.83	1.23	0.98	1.07	0.65
2 ECAP passes (Route A)	0.32	0.76	0.33	0.54	0.44
2 ECAP passes (Route C)	0.10	0.43	0.38	0.34	0.19
4 ECAP passes (Route A)	0.08	0.30	0.29	0.24	0.12
4 ECAP passes (Route C)	0.63	0.41	0.22	0.42	0.02
1 ECAP pass + Annealed 400 °C/15 min	0.92	0.89	0.90	0.90	0.04
4 ECAP passes (Route A) + Ann. 400 °C/15 min	0.35	0.63	0.55	0.54	0.18
4 ECAP passes (Route C) + Ann. 400 °C/15 min	0.41	0.40	0.48	0.43	0.04

[a] $\bar{r} = (r_0 + 2r_{45} + r_{90})/4$; $\Delta r = (r_0 - 2r_{45} + r_{90})/2$

Plastic anisotropy

The values of the average normal anisotropy, $\bar{r}$, and planar anisotropy, Δr, are given in the Table 4 for the starting (annealed), ECAP-processed, and ECAP-processed-and-annealed AA5005 samples. The results revealed that one ECAP pass significantly increased the normal anisotropy to a value greater than unity, which is uncommon for aluminium sheet alloys. Additional ECAP passes resulted in an opposite effect on the normal plastic anisotropy, reducing $\bar{r}$ to the initial (as-annealed) level and even lower values. By contrast, the planar anisotropy increased after one pass, but then steadily improved (i.e., decreased) with the number of passes. Especially significant decreases were observed for two or four passes via route C. Short-time, high-temperature annealing (400 °C/15 min) after one ECAP pass was not detrimental to the normal plastic anisotropy, but reduced Δr to almost zero. A similar effect was observed with annealing after four passes. However, the average normal plastic anisotropy was low after four-pass deformation and annealing did not improve it. Overall, the optimal combination of normal and planar anisotropy was obtained for samples annealed after one ECAP pass.

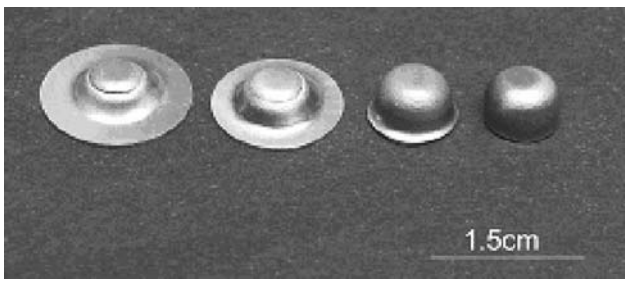

Fig. 10 Cups drawn from blanks of four different diameters

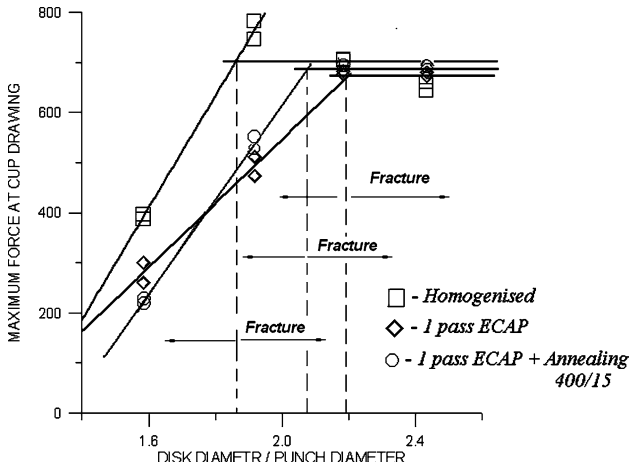

Fig. 11 Swift-cup results for the starting (annealed) material and material given one ECAP pass or one ECAP pass followed by annealing at 400 °C for 15 min

Deep-drawing behavior

Typical observations from the deep-drawing experiments used to establish the effect of ECAP on the limiting-drawing ratio (LDR) are shown in Fig. 10. The deep-drawing results (Fig. 11) indicated that the drawing ratio at which fracture occurred (vertical broken lines) increased measurably after one ECAP pass, confirming an improvement in deep drawability due to increased $\bar{r}$ value (Table 4). However, a reduction in deep drawability was observed after two or four ECAP passes (Table 5), as could be expected from the plastic anisotropy results as well.

The short anneal at 400 °C after one pass did not noticeably affect the gain in deep drawability. Similar annealing after four passes via routes A or C improved the drawability to a modest extent compared to the LDRs of the corresponding as-deformed conditions. Therefore, the optimal deep drawability was obtained for samples after one ECAP pass with or without the final anneal. No earring was observed on the annealed

Table 5 LDR (blank diameter/punch diameter) measurements

Conditions	Annealed (540°/15h)	1p	2p (RA)	2p (RC)	4p (RA)	4p (RC)	1p + Ann. (400°/15)	4p (RA) + Ann. (400°/15)	4p (RC) + Ann. (400°/15)
D/*d*	1.85	2.19	1.92	1.86	1.84	1.82	2.08	2.11	1.99

for the one-ECAP-pass material. Furthermore, no earring was observed for material given one ECAP pass and annealed. These results are thus consistent with the measured values of $\bar{r}$ and Δr (Table 4).

Texture evolution

Texture evolution of AA5005 sheet after one pass of ECAP

Figure 12 compares the {100} PF of primarily annealed sheet (Fig. 12a) with samples processed by one pass of ECAP without (Fig. 12b) and with (Fig. 12c) short high temperature annealing rotated to the TD view. A {111} PF showing the ideal orientations (symbols) and partial fibres (thick solid lines) after a single pass of ECAP of FCC materials with a 90° die is shown in Fig. 12d. From the {100} PF primarily annealed material it is clear that the main texture component present is the cube {001}<100> component. A direct comparison of the {111} PFs and ODFs associated with ideal ECAP one pass through the 90° die (Fig. 12b) and that obtained in our experiments reveals that the three fibers (f_1, f_2 and f_3) characteristic of ideal ECAP after one pass are present [5, 6]. The distribution of orientations ($A^*_{1\theta}$, $A^*_{2\theta}$, $A_\theta/\overline{A_\theta}$, $B_\theta/\overline{B_\theta}$ and C_θ) along these three fibers differ from the ideal ECAP (one pass, 90° die) by only a few degrees of variation. The major intensities were found to be the C_θ and $A^*_{1\theta}$ orientations. Both of these components of the f_2 fiber suggest a relatively strong presence of the f_2 fiber after a single pass. The $A^*_{2\theta}$ orientation was observed to be the weakest among the orientations identified. Since the ideal {111} PF for ECAP after one pass was derived from those associated with ideal negative simple shear after a 45° CCW rotation about the TD, it confirms that the simple shear deformation

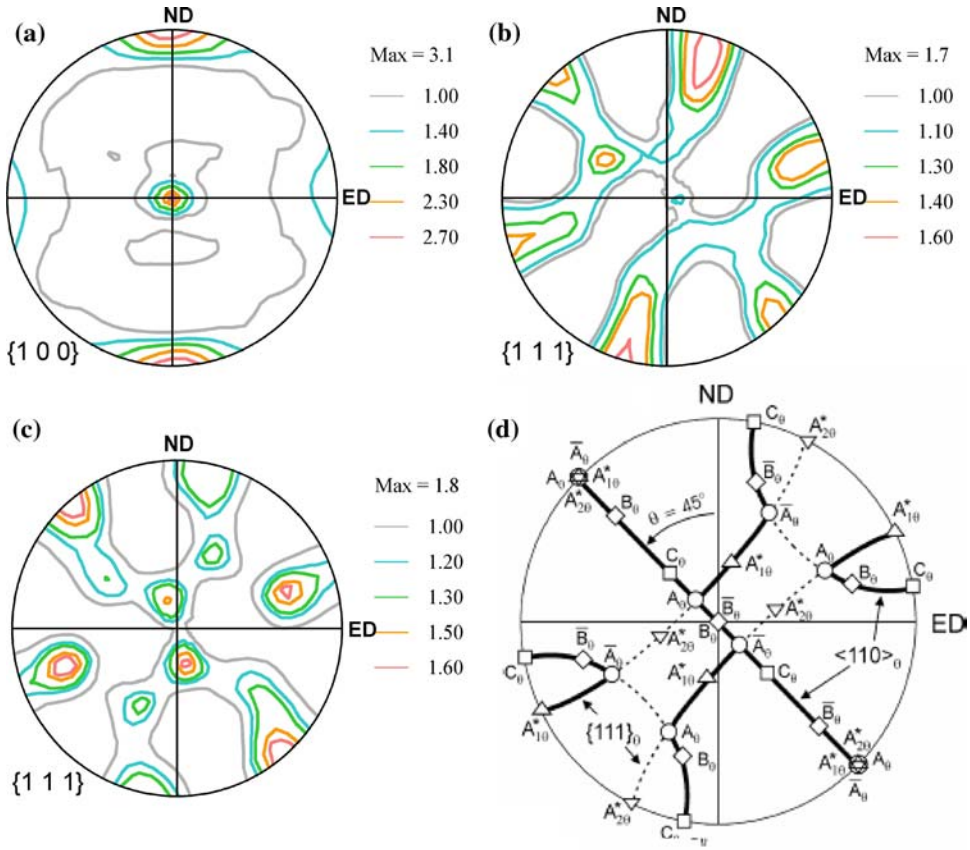

Fig. 12 PFs of AA5005 sheet material: (**a**) Starting (annealed) material, (**b**) after one ECAP pass, and (**c**) after one ECAP pass followed by annealing (400 °C/15 min). The ideal texture components (symbols) and partial fibers (thick solid lines) developed during one ECAP pass [7] are shown in the {111} PF in (**d**)

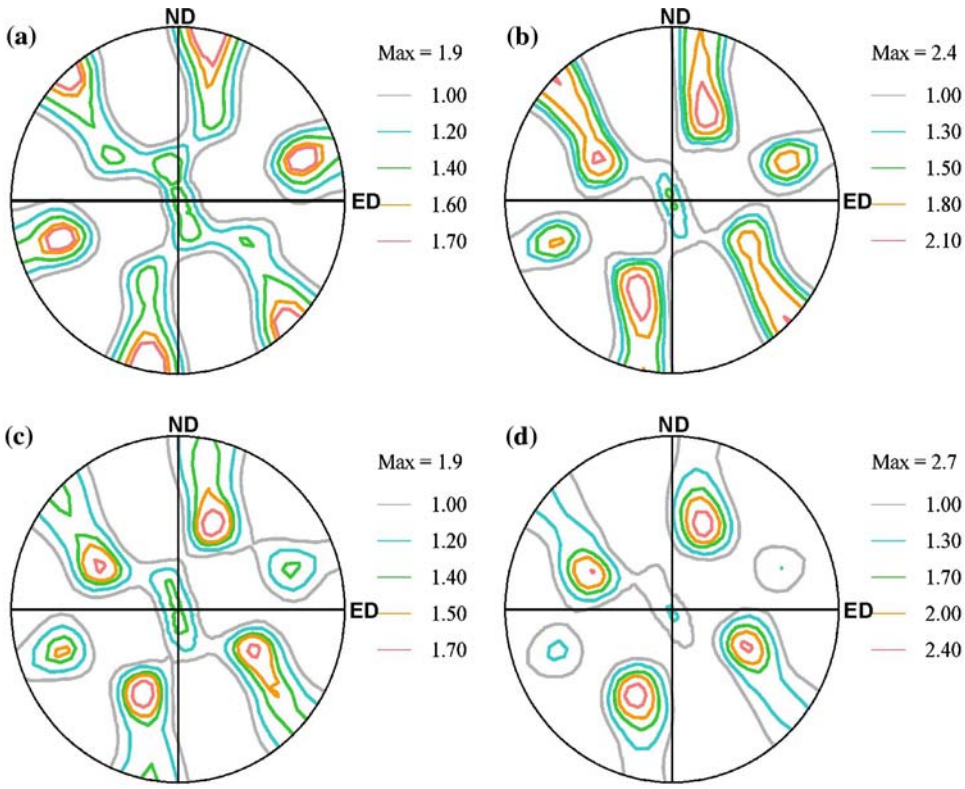

Fig. 13 {111} PFs of AA5005 sheet material after four ECAP passes via (**a**) route A, (**b**) route C, (**c**) route A followed by a 400 °C/15 min anneal, or (**d**) route C followed by a 400 °C/15 min anneal

mode has been realized in the continuous ECAP sheet machine used in these experiments. When the as-processed (Fig. 12b) and annealed (Fig. 12c) material {111} PFs were compared, it was found that the main components of ideal negative simple shear are still present, with similar maximum intensities. However, a slight increase in strength of the conventional recrystallization rolling textures (i.e. the cube {001}‹100›, Goss {011}‹100› and r-cube {013}‹100› components) was observed and accounts for the slight increase in maximum strength.

Because the ideal {111} PF for ECAP after one pass is associated with ideal simple shear after a 45° CCW rotation about the TD, the present texture measurements indicated that a simple shear mode of deformation is indeed obtained during the continuous ECAP processing of sheet reported herein. Furthermore, a comparison of the PFs of the as-processed (Fig. 12b) and the ECAP'ed-and-annealed (Fig. 12c) materials showed that the main components of the ideal simple shear texture were present in both with similar maximum intensities. The increase in $\bar{r}$ following one-pass ECAP (with or without subsequent annealing) can thus be ascribed to the elimination of cube texture and the development of a very weak (almost random) shear texture.

Texture after four ECAP passes

Figure 13 shows the {111} PFs obtained after four ECAP passes via route A (Fig. 13a) and route C (Fig. 13b) as well as after subsequent annealing at 400 °C for 15 min (Fig. 13c, d). The three fibers (f_1, f_2, and f_3) and orientations distributed along these fibers characteristic of ECAP textures are still present with a very modest increase in overall texture strength. The $A^*_{1\theta}$ and $B_\theta/\bar{B}_\theta$ and C_θ orientations were the dominant orientations present along the three fibers for both routes A and C, but were weaker in the case of route C.

Compared with the material given a single ECAP pass, the intensity of the $A^*_{1\theta}$ and $B_\theta/\bar{B}_\theta$ and C_θ orientations *increased* by a maximum of ~1 (× random) after four passes (route A), but underwent very little texture change when using route C. The $A^*_{2\theta}$ and $A_\theta/\bar{A}_\theta$ orientations weakened slightly for both routes. After annealing, a weakening of all orientations along all the three fibers was observed for both routes thus giving rise to incomplete fibers. The $A^*_{2\theta}$ orientation and $A^*_{2\theta}$, $A_\theta/\bar{A}_\theta$, C_θ orientations were completely eliminated in the case of routes A and C, respectively. Despite the similarity of the textures for the single and multi-pass ECAE trials, it is unclear why the $\bar{r}$ values are different, thus warranting further research.

Conclusions

The potential of ECAP processing of sheet material to refine the grain size, enhance mechanical properties, and improve deep drawability was determined for a representative aluminum alloy, AA5005. It was established that only one ECAP pass is required to obtain a significant improvement in both normal and planar anisotropy. A subsequent short-time, high-temperature anneal enabled the recovery of ductility of the material lost during ECAP while maintaining the improved plastic anisotropy. On the other hand, an increase in the number of ECAP passes was detrimental to the mechanical properties and formability despite the increased grain refinement.

Acknowledgement The authors also gratefully acknowledge the support provided by the Air Force Office of Scientific Research and its Asian Office of Aerospace Research and Development (Drs. Ken Goretta, J.P. Singh and J.S. Tiley, program managers).

References

1. Proceedings, NanoSPD Conference, September 2005, Japan, Materials Science Forum, vol 503–504 (2006). Trans Tech Publications, Switzerland
2. Rhee KH, Lapovok R, Thomson PF (2005) JOM 57(5):62
3. Choi C-H, Kim K-H, Lee DN (1998) Mater Sci Forum 273–275:391
4. Tung LK, Quadir MZ, Duggan BJ (2003) Key Eng Mater 233–236:437
5. Li S, Beyerlein I, Bourke MAM (2005) Mater Sci Eng A 394:66
6. Li S, Beyerlein IJ, Alexander DJ, Vogel SC (2005) Acta Mater 53:2111
7. Polmear IJ (1989) Light alloys metallurgy of the light metals second edition. Edward Arnold, London, p 278
8. Iwahashi Y, Horita Z, Nemoto M, Langdon TG (1998) Acta Mater 46:3317